ARTICLE

ACS chemical biology

Mechanistic and Structural Basis of Stereospecific Cβ-Hydroxylation in Calcium-Dependent Antibiotic, a Daptomycin-Type Lipopeptide

Matthias Strieker, Florian Kopp, Christoph Mahlert, Lars-Oliver Essen*, and Mohamed A. Marahiel*

Department of Chemistry/Biochemistry, Philipps University of Marburg, Hans-Meerwein-Strasse, D-35032 Marburg, Germany

ABSTRACT Non-ribosomally synthesized lipopeptide antibiotics of the daptomycin type are known to contain unnatural β-modified amino acids, which are essential for bioactivity. Here we present the biochemical and structural basis for the incorporation of 3-hydroxyasparagine at position 9 in the 11-residue acidic lipopeptide lactone calcium-dependent antibiotic (CDA). Direct hydroxylation of L-asparagine by AsnO, a non-heme Fe^{2+}/α-ketoglutarate-dependent oxygenase encoded by the CDA biosynthesis gene cluster, was validated by Fmoc derivatization of the reaction product and LC/MS analysis. The 1.45, 1.92, and 1.66 Å crystal structures of AsnO as apoprotein, Fe^{2+} complex, and product complex, respectively, with (2*S*,3*S*)-3-hydroxyasparagine and succinate revealed the stereoselectivity and substrate specificity of AsnO. The comparison of native and product-complex structures of AsnO showed a lid-like region (residues F208–E223) that seals the active site upon substrate binding and shields it from sterically demanding peptide substrates. Accordingly, β-hydroxylated asparagine is synthesized prior to its incorporation into the growing CDA peptide. The AsnO structure could serve as a template for engineering novel enzymes for the synthesis of β-hydroxylated amino acids.

In the past decades, the increase of microbial resistance to conventional antibiotics has driven researchers to explore alternatives. Secondary metabolites produced by large, multimodular non-ribosomal peptide synthetases (NRPSs) of bacteria and filamentous fungi had proven to be a reasonable source (*1, 2*). Promising candidates for new antibiotics within this large group of NRPS products are the acidic lipopeptides (*3*). In 2003, a member of this class, daptomycin (*4*), produced by *Streptomyces roseosporus*, was approved for clinical treatment of a wide array of infections caused by Gram-positive bacteria, including methicillin-resistant *Staphylococcus aureus* and vancomycin-resistant enterococci (*5*). Another highly related acidic lipopeptide, similar to daptomycin, is the calcium-dependent antibiotic (CDA), which is non-ribosomally produced by *Streptomyces coelicolor* A3(2) (*6*). CDA (Figure 1) is an undecapeptide lactone that, in addition to an *N*-terminal 2,3-epoxyhexanoyl side chain, contains several D-configured and non-proteinogenic amino acids, including D-4-hydroxyphenylglycine (Hpg), L-3-methylglutamic acid (mGlu), (*Z*)-2,3-dehydrotryptophan, D-3-hydroxyasparagine (D-hAsn), or in some derivatives, D-3-phosphohydroxyasparagine (*7*).

In general, the incorporation of unnatural amino acid building blocks is a key structural feature of NRPS products. This diverse set of monomers is produced either *in cis* on the NRPS assembly line by internal domains, which are part of the multienzyme complex, or *in trans* by so-called NRPS-associated tailoring enzymes (*8*). In the case of CDA, the gene SCO3236 was found by annotation of the CDA biosynthesis gene cluster (*9*) to en-

*Corresponding authors, marahiel@chemie.uni-marburg.de or essen@chemie.uni-marburg.de.

This paper contains web-enhanced objects.

Received for review January 16, 2007 and accepted February 10, 2007.

Published online March 16, 2007

10.1021/cb700012y CCC: $37.00

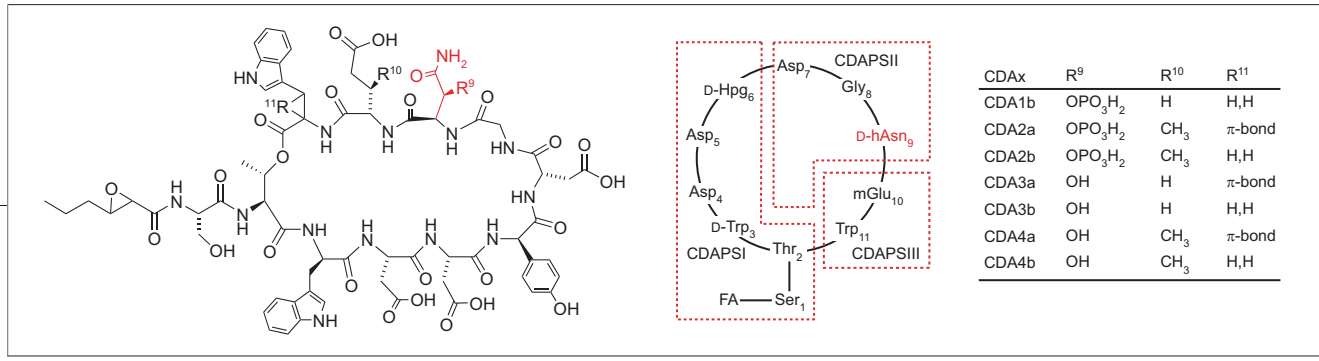

CDAx	R^9	R^{10}	R^{11}
CDA1b	OPO_3H_2	H	H,H
CDA2a	OPO_3H_2	CH_3	π-bond
CDA2b	OPO_3H_2	CH_3	H,H
CDA3a	OH	H	π-bond
CDA3b	OH	H	H,H
CDA4a	OH	CH_3	π-bond
CDA4b	OH	CH_3	H,H

Figure 1. Structure of the CDA family of acidic lipopeptides. Seven CDA derivatives were isolated that showed alterations at the amino acid positions 9, 10, and 11 (as stated in the table on the right). Position 9 (marked in red) is hydroxylated in four derivatives, CDA3a, 3b, 4a, and 4b. CDAPSI/II/III = CDA peptide synthetase I/II/III.

code for the putative hydroxylase AsnO and was shown to be involved in the biosynthesis of CDA (*10*). AsnO shares high sequence identity (~33%) to the trifunctional clavaminate synthase (CAS, encoded by *cas1* or *cas2*) from *Streptomyces clavuligerus* that catalyzes specific hydroxylations of a β-lactam precursor (*11*). Both are members of the CAS-like (CSL) superfamily of Fe^{2+}/α-ketoglutarate (αKG)-dependent oxygenases (*12*). The hydroxylation catalyzed by AsnO was believed to occur either post-synthetically on the asparaginyl residue of the CDA peptide (*9*) or on a precursor tethered to a single module. The latter mode of modification is exemplified by the structurally related Fe^{2+}/αKG-dependent halogenase SyrB2, which catalyzes the chlorination of a peptidyl carrier protein (PCP)-bound threonine (*13*). Alternatively, one may postulate that modification occurs on the level of the free amino acid to provide synthetic precursors, as found in the biosynthesis of etamycin (*14*), actinomycin (*15*), or tuberactinomycin (*16, 17*) building blocks.

In this study, we show that AsnO-catalyzed hydroxylations occur neither post-synthetically on the NRPS-released CDA nor on asparagine tethered to the PCP domain of module *9* but on the level of free L-asparagine. Furthermore, crystal structures of AsnO were obtained in its native apo-form and as complexes with Fe^{2+} alone and Fe^{2+} plus succinate and hAsn at 1.45, 1.92, and 1.66 Å resolutions, respectively. The biochemical and structural data show that L-asparagine is stereoselectively converted to (2*S*,3*S*)-3-hydroxyasparagine by the enzyme AsnO in the presence of αKG and Fe^{2+}, thus providing direct evidence of an aliphatic hydroxylase activity for this non-heme Fe^{2+}-enzyme.

RESULTS AND DISCUSSION

Expression and Purification of PCP9 and AsnO. The *pcp9* encoding gene fragment and the *asnO* gene from the CDA-producer strain *S. coelicolor* A(3)2 were expressed in *E. coli* as His_7-tagged fusions and purified as soluble proteins, with yields of 50 mg for PCP9 and 8–10 mg for AsnO per liter of bacterial culture. After Ni-NTA affinity chromatography, SDS-PAGE indicated >99% purity, and protein masses were verified by mass spectroscopy (MS) analysis.

Hydroxylation Activity of AsnO. To evaluate the biological activity of AsnO, the recombinant enzyme was incubated with several possible substrates: a chemoenzymatically synthesized CDA analogue (*18*) with non-hydroxylated asparagine (nhCDA, Supplementary Figure 1), D- and L-asparagine bound to the PCP domain of module *9* (Asn-*S*-PCP) and the free amino acid (L- or D-asparagine). In the presence of Fe^{2+} and αKG, hydroxylation activity was observed exclusively with the L-enantiomer of the free amino acid. In the case of the peptidic substrates nhCDA and Asn-*S*-PCP, hydroxylation could not be detected by HPLC/MS analysis (Table 1). To facilitate identification and detection of the modified amino acid, we derivatized L-asparagine with *9*-fluorenylmethyl chloroformate (Fmoc-Cl) to yield highly fluorescent Fmoc derivatives (*19, 20*). The incubation of L-asparagine with AsnO (Figure 2, red trace) and subsequent derivatization with Fmoc-Cl gave Fmoc-hAsn. Under assay conditions, the conversion was nearly quantitative after 30 min. In the control reaction (Figure 2, blue trace) without enzyme added, only substrate-derived Fmoc-Asn was detected. In addition to HPLC fluorescence detection, MS was carried out to confirm identification. As noted (Figure 2), peak 1 from the HPLC-separated enzymatic reaction workup gave the

TABLE 1. Masses of the possible substrates nhCDA and Asn-*S*-PCP of AsnO before and after the assay

	Mass (Da)	Possible hydroxylation product (Da)	Mass observed after assay (Da)
CDA analogue	1467.3	1483.3	1467.3
L-asparagine-*S*-PCP	12600.0	12616.0	12600.0
D-asparagine-*S*-PCP	12600.0	12616.0	12600.0

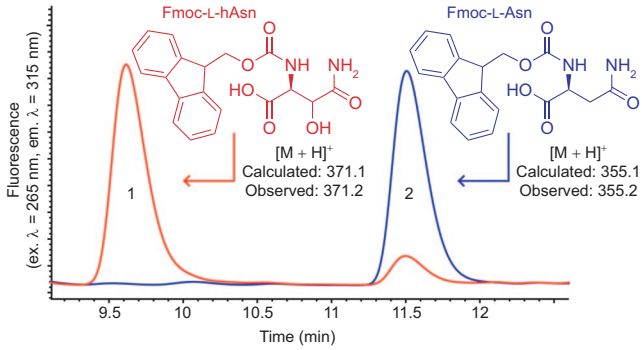

Figure 2. β-Carbon hydroxylation of L-asparagine by AsnO. HPLC traces and mass analyses of Fmoc-derivatized hAsn (peak 1) and L-asparagine (peak 2). The blue and red traces represent the fluorescence signals before and after incubation of L-asparagine with AsnO under assay conditions.

L-hAsn-derived fluorenylmethyl, and peak 2 had the mass of the L-asparagine adduct. The finding that AsnO acts exclusively on free L-asparagine to form hAsn was somewhat unexpected, because it was postulated before that AsnO tailors CDA post-synthetically (*9*). Because AsnO is unable to hydroxylate Fmoc-Asn and the Fmoc derivatization of asparagine and hAsn is completed within a few seconds (*19*, *20*), we stopped the enzyme assay by adding Fmoc-Cl at the appropriate time points. The kinetic parameters of AsnO for L-asparagine hydroxylation were determined to an apparent K_M of 0.479 ± 0.067 mM and k_{cat} of 298.8 ± 19.2 min^{-1}, leading to a catalytic efficiency of $k_{cat}/K_M = 0.62 \pm 0.15$ min^{-1} μM^{-1}. For comparison, other small-molecule hydroxylating non-heme oxygenases, such as the enzyme RdpA from *Sphingomonas herbicidovorans* MH, which catalyzes the oxidative decomposition of 2-(4-chloro-2-methylphenoxy)-propionic acid (K_M = 380 μM, k_{cat} = 252 min^{-1}) (*21*), exert similar catalytic efficiencies.

We also tested other amino acids and asparagine derivatives, including D-asparagine (Supplementary Table 1) for AsnO-mediated hydroxylation by MS analyses, but it became apparent that only L-asparagine is accepted as a cognate substrate for AsnO. In controls, without added αKG or Fe^{2+}, no conversion of L-asparagine was observed.

Interestingly, in mature CDA only D-hAsn, which is generated by the epimerization (E) domain of module 9 (Figure 3), is found. Derivatives of CDA with asparagine instead of hAsn at the canonical position are not observed under fermentation conditions in wild-type strains (*3*) but in Δ*asnO*-deletion mutant strains with decreased CDA production (*10*). Thus, one may postulate that the A domain of module 9 preferably accepts hAsn but is also capable of L-asparagine activation with reduced efficiency. For wild-type strains, the following mode of hAsn incorporation is reasonable: After activation of the amino acid as hAsn-AMP, a thioester with the sulfhydryl group of the PCP-cofactor 4′phosphopantheteine could be formed. The PCP domain then would transfer hAsn to the E domain, where it is converted from the 2*S*,3*S* to the 2*R*,3*S* configuration. After that, the latter one would be accepted by the neighboring condensation domains, which catalyze the peptide bond formations. Subsequent chain elongation and product release would yield naturally occurring CDAs with hydroxylated D-asparagine moieties at position 9 of the peptide backbone (Figure 3).

Overall Structure Description. Trigonal crystals of AsnO were grown within 2 d and found to comprise one AsnO molecule per asymmetric unit. The crystal structure of AsnO was solved at 1.45 Å resolution by molecular replacement, using the related structure of CAS (*22*) as a search model. Like other members of the CSL superfamily, the refined structure of AsnO contains a core of nine β-strands (A–I), eight of which are folded into a jelly roll topology, building a major and a minor sheet with five (B, G, D, I, and C) and three β-strands (F, E, and H), respectively (Figure 4, panel a). The jelly roll fold is sandwiched between two, largely α-helical sub-

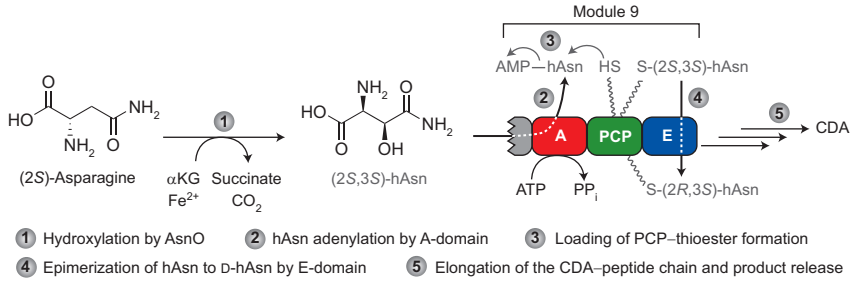

Figure 3. Scheme showing the reaction sequence during the biosynthesis of cyclic CDA peptides bearing β-hydroxylated asparagines at position 9.

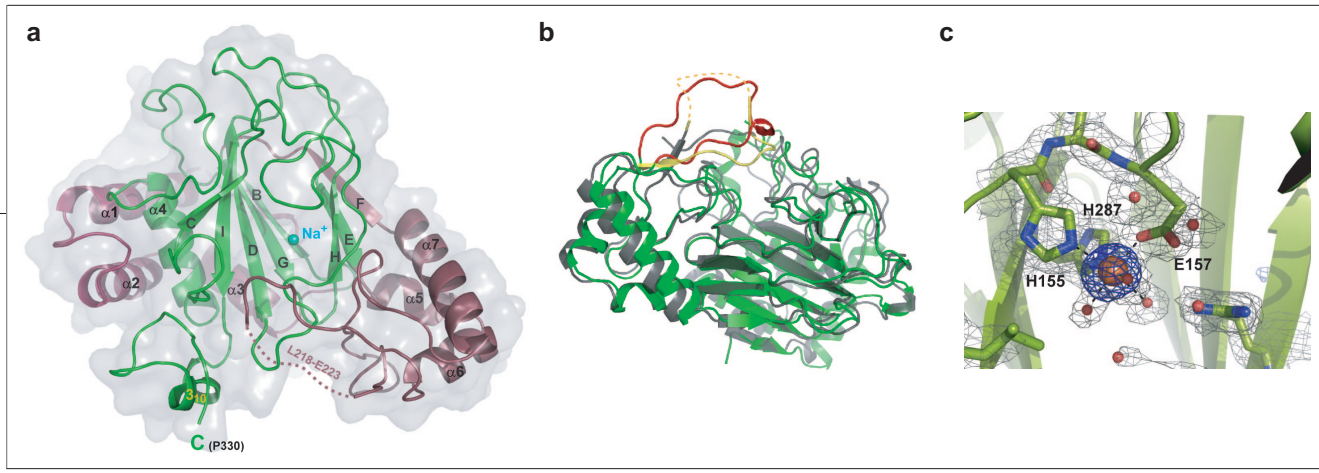

Figure 4. Crystal structure of AsnO. a) Overall structure of the apo-form of AsnO with β-strands B, G, D, I, and C building the major side and β-strands F, E, and H building the minor side of the jelly roll fold. Seven α-helices, one 3_{10}-helix, and one additional β-strand (A) complete the structure. b) Comparison of the structure of the AsnO·Fe(II) complex (green) with CAS (PDB accession code 1DRY) (gray). A dashed line indicates the disordered region (residues G208–A214) of CAS. (c) SIGMAA-weighted $2F_{obs} - F_{calc}$ electron density showing the binding of an iron ion to the active site of AsnO (contouring level 1 $\sigma \equiv 0.11$ e$^-$/Å^3). Anomalous difference electron density for the iron atom is shown in blue (contouring level 5 $\sigma \equiv 0.06$ e$^-$/Å^3, $\lambda_{Xray} = 1.54179$ Å).

Ⓦ View Figure 4, panel a and Figure 4, panel b in 3D. See a fully interactive version in the *ACS Chemical Biology* 3D Molecular Viewer in Jmol on the journal web site. In addition, you can explore this structure by using FirstGlance in Jmol.

domains: an *N*-terminal region (residues S10–G71) containing three helices (α1–α3), with an adjacent β-strand (A) parallel to the first β-strand B of the jelly roll fold, and an extended insertion (residues V188–P274) containing helices α5–α7, which links the fourth (E) and fifth (F) β-strand of the jelly roll fold. Two flexible loop regions border the active site (residues V135–P165 and A205–T249), and near the *C*-terminus a 3_{10}-helix (residues L312–M318) is found.

In the active site region of the native AsnO, the electron density reveals an ion that is octahedrally coordinated to the residues H155, E157, and H287, in addition to three water molecules. As the result of a lack of sufficient electron density and anomalous signal, this ion was assigned as a sodium ion rather than an Fe^{2+} ion. Accordingly, the hydroxylation activity of recombinant AsnO strictly depended on exogenously added Fe^{2+} ions in the enzyme assay.

In further studies, the crystal structure of AsnO with the Fe^{2+} cofactor bound was solved at 1.92 Å resolution by soaking AsnO crystals under anaerobic conditions with Fe^{2+} and αKG. This AsnO·Fe^{2+} complex is almost identical to the apo-form, except that for the central ion no additional electron density for αKG was observed. Comparison of CAS (*22*) and AsnO (Figure 4, panel b) shows the high structural similarity of these two enzymes with an overall root mean square deviation of 1.3 Å for 257 Cα-positions.

The residues H155, E157, and H287 form the conserved HXD/E . . . H iron binding motif (Figure 4, panel c) that is located at the mouth of the minor β-sheet, near and within β-strand H. The histidine and acidic residues of this motif are located within the first flexible loop between β-strands C and D of the jelly roll fold, whereas the distal histidine, H287, is positioned on β-strand H. The same metal coordinating triad is conserved in almost all characterized non-heme iron-dependent oxygenases, including those with folds different from αKG-dependent oxygenases (*12, 23*).

This iron-binding motif, which projects from the rigid β-barrel core of the Fe^{2+}/αKG-dependent oxygenases, fulfills a role similar to that of the porphyrin ring in cytochrome P450 enzymes, which is a stable platform to ligate the iron and the subsequently formed reactive intermediates. The presence of a jelly roll topology in AsnO like those in CAS (*22*), isopenicillin N synthase (*24*), and deacetoxycephalosporin C synthase (*25*), in which active site residues are located on analogous strands of the core domain, implies a divergent evolutionary relationship between AsnO and other members of the extended family of αKG/Fe^{2+}-requiring and related enzymes, *e.g.*, the halogenase SyrB2 (*13*).

Active and Substrate Binding Site of AsnO. Crystals soaked with the substrate L-asparagine and Fe^{2+}-cofactor/αKG-cosubstrate led to the structure of a product complex comprising iron either in the Fe^{2+} or Fe^{3+} state, (2*S*,3*S*)-3-hydroxyasparagine, and succinate, instead of the expected educt complex. Most likely, after removal of the crystals from the anaerobic chamber, the short exposure of the crystals (~30 s) to atmospheric oxygen for flash freezing caused rapid formation of the product complex.

The hAsn is intimately bound within the active site, and the C3 hydroxy group can be clearly assigned by electron density at 1.66 Å resolution to correspond to the pro*S*-hydrogen of the L-asparagine substrate. Its coordination to the catalytic iron (Figure 5, panel a) suggests that the educt asparagine is similarly bound to

the active site with its pro*S*-hydrogen located next to the reactive oxygen of the ferryl species. Thus, we anticipate that this hydrogen atom is abstracted during hydroxylation with retention of configuration to give 2*S*,3*S*-hAsn. This is consistent with the observation that both heme- and non-heme-dependent hydroxylases typically affect hydroxylation of unactivated methylene groups, with retention of stereochemistry (*26*). Furthermore, hAsn and, as anticipated, the L-asparagine substrate is bound by seven amino acids of the peptide backbone (Figure 5, panel b). The α-carboxy group of hAsn forms a salt bridge with R305 and hydrogen bonds to N146 and the peptide group preceding this residue. The α-amino group forms another salt bridge to E125 and is also bound by one oxygen atom of the carboxyl group of the iron binding E157 side chain. The carboxamide group of the side chain of hAsn participates in hydrogen bonds with N158, D241, and *via* a water molecule the peptide group of Q144 (Figure 5, panels a and b). As found by a BLAST search with the entire AsnO sequence as the query, AsnO shares high sequence homology with several putative as well as biochemically characterized non-heme Fe^{2+}/αKG oxygenases, which participate in the biosynthesis of NRPS products. On the basis of the AsnO crystal structure of the product-bound state, five proteins exhibiting the greatest similarity were selected to generate 3D-homology models with MODELLER7 (*27*) (not shown). These are the putative proteins SCO2693 (*28*) (57% identity), produced by *S. coelicolor*, LptL (*29*) (45%) from *S. roseosporus*, TobO (*30*) (37%) from *Streptomyces* sp. DSM 40477, and the biochemically exam-

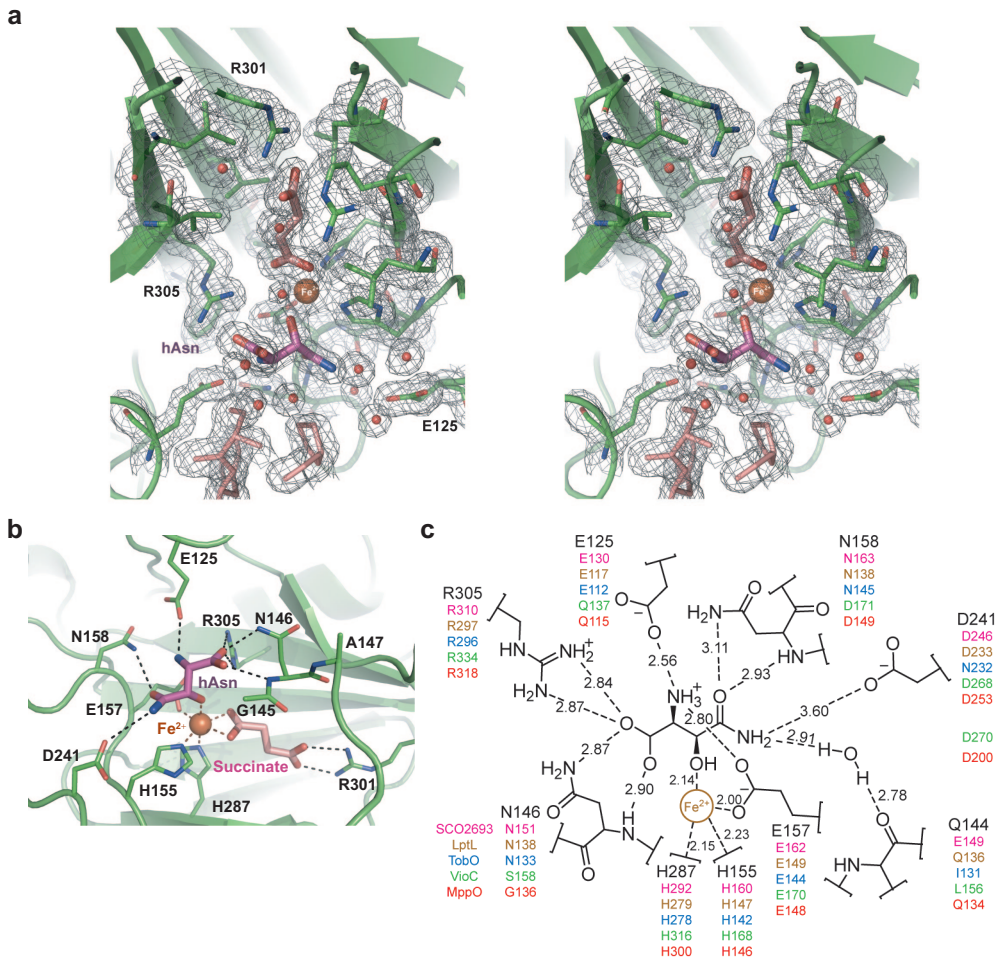

Figure 5. Active site in the AsnO·Fe(II)·succinate·hAsn complex. a) A stereo diagram shows the $2F_{obs} - F_{calc}$ electron density for the active site (contouring level 1.0 σ ≡ 0.24 e^-/Å^3). The coordination of the reaction products (2*S*,3*S*)-3-hydroxyasparagine and succinate to the catalytic iron atom allows unambiguous assignment of the stereochemistry of the hydroxylated asparagine. b) Product–enzyme interactions within the active site. The succinate molecule forms a salt bridge to the conserved arginine R301. The reaction product (2*S*,3*S*)-3-hydroxyasparagine is coordinated to the active site iron *via* its β-hydroxy group and forms seven additional interactions with the protein scaffold (see text for details). c) Schematic representation of hAsn–AsnO interactions and homologous enzymes. The (2*S*,3*S*)-3-hydroxyasparagine interactions with the protein scaffold are represented (black; see text for details). 3D-Homology models (*27*) (not shown) based on the AsnO product complex revealed the substrate binding residues of SCO2693 (*28*) (magenta), LptL (*29*) (brown), TobO (*30*) (blue), VioC (*17*) (green), and MppO (*31*) (red). These are stated below the corresponding AsnO residues. Additional putative substrate binding residues of VioC and MppO could be found on the right side.

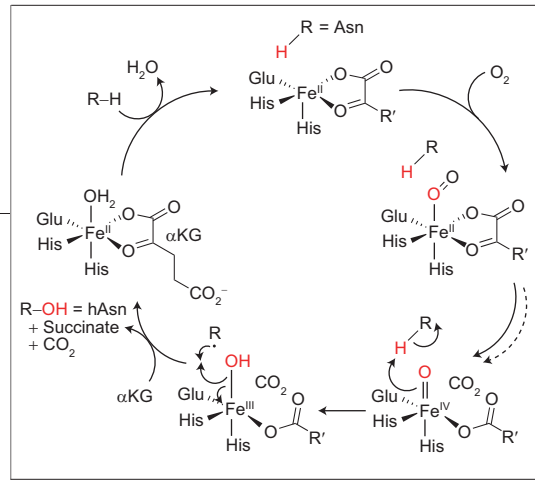

Figure 6. Proposed mechanism of asparagine hydroxylation by AsnO. A highly reactive ferryl species, generated by decomposition of αKG to succinate, deprotonates the β-CH_2 group of asparagine, yielding substrate and Fe(III)-OH radicals. Recombination restores the Fe^{2+} oxidation state and leads to the hydroxylated asparagine.

ined enzymes VioC (*17*) (33%) as well as MppO (*31*) (31%) produced by *Streptomyces vinaceus* and *Streptomyces hygroscopicus*, respectively. Strikingly, most of the α-carboxy and α-amino group binding residues are conserved in the 3D-homology models for all five proteins.

In the case of SCO2693 and LptL (Figure 5, panel c; residues in magenta and brown), all residues are conserved, except Q144, which is a glutamate in SCO2693. Because this residue is only indirectly involved in substrate binding *via* its peptide group, one can predict that both enzymes will also use L-asparagine as a substrate for the generation of (2*S*,3*S*)-3-hydroxyasparagine. For LptL, this finding perfectly agrees with the prediction that it is involved in the hAsn precursor synthesis for the lipopeptide antibiotic A54145, which bears an hAsn moiety at position 3 of the peptide backbone (*3, 29*). *TobO*, which is part of the aminoglycoside tobramycin biosynthesis cluster (*30*), may encode for a protein involved in the synthesis of hydroxylated precursors or inhibitors for this antibiotic. To our knowledge, nothing is known about a possible substrate. Compared with AsnO, TobO (Figure 5, panel c; residues in brown) notably differs only in the acidic D241 residue, which is changed to N232. Thus, we predict that TobO catalyzes the oxygenation of substrates with an acidic side chain, such as aspartic acid or glutamic acid. It was shown that VioC selectively catalyzes the formation of (2*S*,3*S*)-3-hydroxyarginine with L-arginine as a substrate during viomycin biosynthesis (*17, 32*). The model (Figure 5, panel c; residues in green) revealed that Q137, which corresponds to α-amino group binding E125 in AsnO, rather binds the α-carboxy group and the side chain of D171, which is positioned analogously to the carbonyl group binding the N158 residue of AsnO, the α-amino group. The D241 residue is conserved (D268) and could establish a salt bridge with the guanidinium group of the L-arginine substrate. Furthermore, an additional acidic residue (D270) in proximity to the substrate may stabilize the basic arginine side chain. Finally, MppO (*31*) catalyzes the hydroxylation of the arginine-derived unnatural amino acid enduracididine at the β-position to generate (2*S*,3*S*)-3-hydroxyenduracididine building blocks for the biosynthesis of the potent glycopeptide antibiotics mannopeptimycins. The MppO model (Figure 5, panel c; residues in red) showed high similarity to VioC, and the α-carboxy and α-amino group should be bound identically. The side chains of D253 (correspondent to D241 in AsnO) and of the additional acidic residue D200 should bind the cyclic guanidinium group and thereby stabilize enduracididine in the substrate binding pocket.

Furthermore, the second reaction product, succinate, is bound by AsnO *via* a salt bridge to the guanidinium group of the conserved residue R301 that is similarly formed in other structures of αKG/Fe^{2+}-dependent oxygenases complexed to αKG. This arginine is usually found 14–22 residues after the conserved second histidine residue of the iron binding motif (*12*). In all 3D-homology models, this arginine is highly conserved, located exactly 14 residues after the second iron binding histidine.

The high number of specific interactions between the protein scaffold of AsnO and L-asparagine rationalizes why the enzyme exclusively catalyzes the hydroxylation of L-asparagine and why the product has to be 2*S*,3*S*-configured. The 3D-homology models based on the product complex of AsnO share this high quantity of specific interactions with their substrates and explain the observed 2*S*,3*S*-stereoselectivity for the hydroxylation product in the case of MppO (*31*). Furthermore, AsnO could be used as an archetype for putative non-heme Fe^{2+}/αKG-dependent oxygenases that are involved in the generation of β-hydroxylated amino acid building blocks for NRPS products as exemplified by 3D-homology models of SCO2693 (*28*), LptL (*3, 29*), and VioC (*17*).

Catalysis. Like other members of the Fe^{2+}/αKG-dependent oxygenases (*12, 23*), AsnO decarboxylates αKG by utilizing dioxygen to generate carbon dioxide, succinate, and a reactive oxidizing species that mediates substrate oxidation (Figure 6). One of the oxygen atoms from O_2 is incorporated into succinate, and the other into the alcohol of the product. It is proposed (*12, 23*) that after substrate binding Fe^{2+} and oxygen react to give a Fe(III)-superoxo species, the anion of which attacks the 2-ketogroup of αKG, which is activated by the

Lewis acidity of the iron. This reaction leads to a persuccinate species, and after its collapse, to a potent Fe(IV)=O species, which in turn abstracts a hydrogen radical from the substrate asparagine β-CH_2 group. This results in a Fe(III)-OH and the substrate radical in proximity to each other in the active site. Radical recombination involves $OH^{\cdot}$ transfer to the substrate radical, yielding the observed alcohol product and regenerating the starting Fe^{2+}-oxidation state (Figure 6). The key to the catalytic strategy is the generation of the high-valent oxoiron (Fe(IV)=O) species that removes a hydrogen atom from even the most unactivated carbon sites of a bound substrate (*33, 34*).

Lid Closure. The biochemical characterization of AsnO showed that AsnO hydroxylates neither a CDA analogue with unmodified Asn-9 nor PCP-bound asparagine. The active site of AsnO is canopied by a flexible lid region (residues F208–E223) that is partly disordered in the apo-form (Figure 4, panel a; residues L218–E223), but becomes ordered upon complexation of iron in the AsnO·Fe^{2+} complex (Figure 4, panel b, in green), albeit with high overall B-factors. In the case of CAS (*22*), this loop region remains partly disordered (Figure 4, panel b) in the complex with Fe^{2+}, αKG, and *N*-α-L-acetylarginine, the stable analogue of the monocyclic β-lactam hydroxylation substrate. Interestingly, the product complex shows a product-induced structural change for this lid region (Figure 7, panel a) that causes almost complete shielding of the products from bulk solvent access. The three abreast proline residues (P212–214) build a hydrophobic wedge (Figure 7, panel b) that seals the active site. The interaction between the carboxyl group of the E125 side chain and the α-amino group of bound asparagine might be crucial to orient E125 in such a way that it establishes a hydrogen bond with the hydroxy group of the side chain of S215 (Figure 7, panel b). Thus, the lid closes concomitantly with L-asparagine substrate binding. To our knowledge, such a substrate induced-fit mechanism, explaining the high substrate specificity of AsnO, was not observed before in the CSL superfamily of Fe^{2+}/αKG-dependent oxygenases.

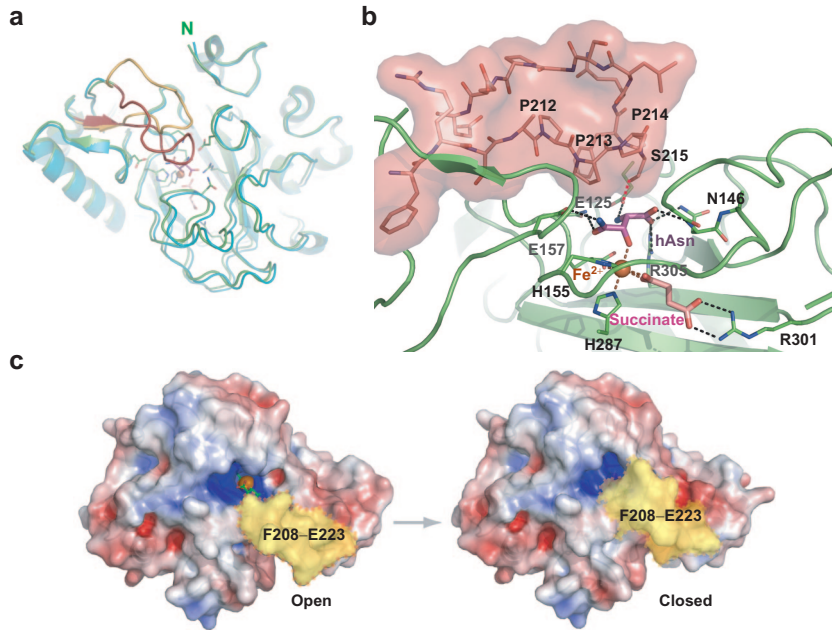

Figure 7. Lid closure of AsnO upon substrate binding. a) Structural comparison between the product-bound AsnO·Fe(II)·succinate·hAsn complex (green) and the AsnO·Fe(II) complex (cyan). The lid region (F208–E223) is marked in red and orange. b) Sealing of the active site by the lid region. The residue E125 that binds to the α-amino group of the substrate L-asparagine is favorably positioned by forming a hydrogen bond with the side chain of S215, projecting from the lid region. c) Electrostatic representation of the open and closed state of AsnO as calculated by APBS (blue, +5 kT/e; red, −5 kT/e; ion concentration 0.1 M). In the open state, the lid region (accentuated in yellow) keeps the active site accessible for the binding of substrate and cosubstrates. Concomitant with substrate binding, the lid mostly occludes the active site (right side) from bulk solvent. For clarity, the reaction products are shown as green sticks around the catalytic iron cofactor (orange).

Ⓦ View Figure 7, panel a, Figure 7, panel b, and Figure 7, panel c in 3D. See a fully interactive version in the *ACS Chemical Biology* 3D Molecular Viewer in Jmol on the journal web site. In addition, you can explore this structure by using FirstGlance in Jmol.

In the AsnO·Fe^{2+} structure, without αKG or asparagine bound, the lid-like region F208–E223 is open and leaves the enzyme center accessible for binding of substrate and cosubstrate. With the bound products, hAsn and succinate, the lid bends toward the product binding site, burying it completely inside the enzyme (Figure 7, panel c). Sterically demanding peptidyl-asparagine substrates could either not bind to the active site or not trigger the lid closure. Thus, it could be concluded that these compounds are incapable of accessing the active site, and only the free amino acid will be hydroxylated. That is quite the contrary to factor inhibiting HIF-1 (FIH-1) (*35*), which hydroxylates a conserved asparaginyl residue in the master switch of cellular hypoxia re-

sponses, hypoxia-inducible factor 1 (HIF-1), under normoxia, which suppresses the transcriptional activity of HIF-1 (*36*). In FIH-1, the substrate binding site is a large groove (15 Å wide and 40 Å long), providing enough space for the binding of a large α-helical region of HIF-1 (*35*).

Conclusions. As shown above, the tailoring of the ninth residue of the CDA peptide backbone does not take place post-synthetically on the cyclic CDA, as previously postulated (*9*). Furthermore, the tailoring does not occur while asparagine is tethered covalently to a PCP as an asparaginyl-phosphopantheteinyl-thioester, as in the structurally related non-heme αKG halogenase SyrB2 (*13*). Instead, β-hydroxylation occurs on the free amino acid level and resembles the presynthesis of (2*S*,3*S*)-3-hydroxyarginine and (2*S*,3*S*)-3-hydroxyenduracididine by VioC (*17*) and MppO (*31*), which also generate building blocks for the biosynthesis of potent antimicrobial agents. β-Hydroxylated asparagines, aspartates, and other amino acids could be found in several antibiotics (*12, 37, 38*) or pharmacologically relevant agents (*39*), showing their medicinal importance. The insights gained by AsnO structures, which demonstrate how nature stereoselectively synthesizes β-hydroxylated amino acids, a challenging task for the synthetic chemist, will abet in the design and discovery of novel hydroxylases, in order to generate a large pool of these building blocks for the synthesis of various natural products.

METHODS

Strains, Culture Media, and General Methods. The *E. coli* strains were grown in Luria–Bertani medium, supplemented with 100 μg mL^{-1} ampicillin (final concentration). Oligonucleotides were purchased from Operon. DNA dideoxy sequencing confirmed the identity of all plasmids constructed.

Construction of Expression Plasmids. All recombinant gene fragments were amplified by polymerase chain reaction from chromosomal DNA of *S. coelicolor* A3(2) (DSM 40783) by using the Phusion polymerase (Finnzymes). According to the manufacturer's protocols for template DNA with high GC content (*S. coelicolor*, 74%), the dNTP concentration was increased to 20 mM. The *asnO* gene was amplified by using the primer combination of 5′-*asnO* (5′-AAA AAA GGA TCC GCT GCG AAT GCC GCG GG-3′) and 3′-*asnO* (5′-AAA AAA GCG GCC GCT CAG GCG GGC TGC GGG-3′). The gene fragment encoding the PCP of module 9 (fragment of *SCO3231*, *cdaPSII*) was amplified by using the oligonucleotides 5′-*pcp9* (5′-AAA AAA GGA TCC GGC CGG GCC CCG GTC ACG G-3′) and 3′-*pcp9* (5′AAA AAA CTG CAG CTG CGC CTC GGC GAG TTC GA-3′). After purification and digestion with *Bam*HI, *Not*I (*asnO*) and *Bam*HI, *Pst*I (*pcp9*), respectively, the gene fragments were ligated into the corresponding restriction sites of a pQE30-derived vector (Qiagen).

Production of Recombinant Enzymes. pQE30-based cloning products were used to transform *E. coli* BL21(DE3) (Novagen). The transformed cells were grown at 37 °C to an optical density of 0.5 (600 nm), induced with 1 mM isopropyl-β-D-thiogalactopyranoside, and again grown at 30 °C for 3 h. The recombinant proteins were purified by Ni-NTA affinity chromatography (Amersham Pharmacia Biotech). Fractions containing the recombinant proteins were identified by 10% SDS-PAGE analysis, pooled, and subjected to buffer exchange into 25 mM HEPES, 50 mM NaCl, pH 7.0 using HiTrap desalting columns (Amersham Pharmacia Biotech). The concentration of the purified proteins was determined spectrophotometrically using calculated extinction coefficients at 280 nm. After being flash-frozen in liquid nitrogen, the proteins were stored at −80 °C.

Enzyme Assays. *General.* The recombinant AsnO (0.5 μM) was incubated for 30 min at 25 °C with the different substrates (250 μM), the cofactor $(NH_4)_2Fe(SO_4)_2$ (500 μM), cosubstrate αKG (500 μM), and 20 μg of catalase in 50 μL of 50 mM HEPES buffer (pH 7.5). The catalase was added to capture reactive oxygen species to prevent autoxidation of the enzyme. Controls were carried out without either AsnO or Fe^{2+}/αKG, respectively.

Assay with Chemoenzymatically Derived CDA. The CDA analogue, without amino acid modifications, was chemoenzymatically produced as previously described (*18*) and incubated with AsnO (see above). The reaction was stopped by adding 50 μL of a 4% (v/v) TFA solution and then analyzed for possible hydroxylation *via* reversed-phase HPLC/MS analysis on a C18 Nucleodur column (Macherey and Nagel, 250/3, pore diameter of 100 Å, particle size of 3 μm) with the following gradient: 15–60% acetonitrile, 0.1% (v/v) TFA and water, 0.1% (v/v) TFA from 0 to 40 min at 0.3 mL min^{-1} and 45 °C.

Assay with Asn-S-PCP. Recombinant PCP9 (54 μM) was incubated with synthetic coenzyme A (CoA)-Asn-thioester (400 μM) and the 4′-phosphopantheteine transferase (Sfp; 5 μM) for 15 min at 37 °C. The syntheses of CoA-thioesters were carried out as previously described (*40*). Subsequently, the PCP-bound asparagine was incubated with AsnO following the general enzyme assay. Analysis was carried out by high-accuracy MS on an API Qstar Pulsar I device (Applied Biosystems).

Amino Acid Assay. L-Asparagine was incubated with AsnO (see above), and the reaction was stopped by adding Fmoc-Cl solution, as previously described (*20*). The Fmoc-N^{α}-derivatized reaction products were analyzed by HPLC separation and fluorescence detection using a Synergi Fusion-RP column (Phenomenex, C18 polar ec, pore diameter of 80 Å, particle size of 3 μm) with the following gradient: 0–20% eluent B (100% acetonitrile) and eluent A (78% (v/v) 0.1 M aqueous NaOAc solution, 22% (v/v) acetonitrile) in 17 min at 0.3 mL min^{-1} and 17.5 °C. Kinetic parameters K_M and k_{cat} were determined by varying the L-asparagine concentration between 50 and 500 μM and stopping the reaction by addition of Fmoc-Cl solution.

Crystallization, Soaking, and Data Collection. Crystals of AsnO from *S. coelicolor* were grown at 18 °C by the sitting-drop vapor-diffusion method. Native crystals were obtained in 2.5 M sodium acetate, 0.1 M HEPES, pH 4.6, and in 4 M sodium formate at a protein concentration of 8.3 mg/mL in 25 mM HEPES, 50 mM NaCl, pH 7.0. The product complex was achieved by soaking AsnO crystals with degassed 10 mM $(NH_4)_2Fe(SO_4)_2$, 20 mM αKG, and 50 mM L-asparagine-solution for 60 min under protection gas (97% nitrogen, 3% hydrogen) in an anaerobic chamber. Soaking of the AsnO crystals with αKG and Fe^{2+}, under the conditions described above, led to an AsnO·Fe^{2+} com-

plex. Cryoprotection was achieved by washing the crystals in the mother liquor that contained 30% (v/v) glycerol. Intensity data from flash-frozen crystals were collected at beamline X13 at EMBL, Hamburg, Germany at 1.45 Å resolution for the apo-form of AsnO and 1.66 Å for the AsnO·Fe(II)·succinate·hAsn complex. A 1.92 Å dataset for the AsnO·Fe(II) complex was recorded on an in-house Cu Kα rotating anode. Diffraction data were integrated and scaled with the programs MOSFLM and SCALA of the CCP4 program suite (*41*).

Structure Solution and Refinement. The crystal structure of AsnO was solved by molecular replacement using the program MOLREP (*42*) and chain A of the CAS (PDB accession code 1DRY) as a search model. Structure refinement was carried out using REFMAC5 (*43*) and COOT (*44*). The final model of AsnO contains residues S10–P330, but misses a disordered region spanning L218–E223. Anomalous difference electron density maps indicated that no iron atom was bound in the active site. Instead, the octahedrally coordinated ion observed at the iron binding site was assigned as a sodium ion originating from the crystallization buffer.

Anomalous difference electron density maps indicated for Fe^{2+}/αKG-soaked AsnO crystals only the binding of the iron atom to the active site. For data statistics, refer to Supplementary Table 2. PyMOL (*45*) was used to prepare all figures displaying structural information (Figure 4; Figure 5, panels a and b) (*7*).

Accession Codes: Coordinates and structure factors have been deposited in the Protein Data Bank. PDB accession codes: native AsnO, 2OG5; AsnO·Fe^{2+}, 2OG6; AsnO·Fe^{2+}·succinate·hAsn, 2OG7.

Acknowledgments: We gratefully acknowledge U. Linne for carrying out high-resolution MS measurements, S. Shima (MPI for terrestrial microbiology, Marburg, Germany) for providing the anaerobic chamber, M. Hahn for technical assistance, and A. Schmidt for support at beamline X13, EMBL, Hamburg, Germany. We thank the Deutsche Forschungsgemeinschaft and the Fonds der Chemischen Industrie for financial support.

Supporting Information Available: This material is free of charge *via* the Internet.

REFERENCES

1. Walsh, C. T. (2004) Polyketide and nonribosomal peptide antibiotics: modularity and versatility, *Science 303*, 1805–1810.
2. Weber, T., and Marahiel, M. A. (2001) Exploring the domain structure of modular nonribosomal peptide synthetases, *Structure 9*, R3–9.
3. Baltz, R. H., Miao, V., and Wrigley, S. K. (2005) Natural products to drugs: daptomycin and related lipopeptide antibiotics, *Nat. Prod. Rep. 22*, 717–741.
4. McHenney, M. A., Hosted, T. J., Dehoff, B. S., Rosteck, P. R., Jr., and Baltz, R. H. (1998) Molecular cloning and physical mapping of the daptomycin gene cluster from *Streptomyces roseosporus*, *J. Bacteriol. 180*, 143–151.
5. Fraser, T. G., Hansen, C., and Long, J. K. (2006) Newer antibiotics for serious Gram-positive infections, *Clev. Clin. J. Med. 73*, 847–853.
6. Lakey, J. H., Lea, E. J., Rudd, B. A., Wright, H. M., and Hopwood, D. A. (1983) A new channel-forming antibiotic from *Streptomyces coelicolor* A3(2) which requires calcium for its activity, *J. Gen. Microbiol. 129*, 3565–3573.
7. Kempter, C., Kaiser, D., Haag, S., Nicholson, G., Gnau, V., Walk, T., Gierling, K.-H., Decker, H., Zähner, H., Jung, G., and Metzger, J. W. (1997) CDA: calcium-dependent peptide antibiotics from *Streptomyces coelicolor* A3(2) containing unusual residues, *Angew. Chem., Int. Ed. Engl. 36*, 498–501.
8. Walsh, C. T., Chen, H. W., Keating, T. A., Hubbard, B. K., Losey, H. C., Luo, L. S., Marshall, C. G., Miller, D. A., and Patel, H. M. (2001) Tailoring enzymes that modify nonribosomal peptides during and after chain elongation on NRPS assembly lines, *Curr. Opin. Chem. Biol. 5*, 525–534.
9. Hojati, Z., Milne, C., Harvey, B., Gordon, L., Borg, M., Flett, F., Wilkinson, B., Sidebottom, P. J., Rudd, B. A., Hayes, M. A., Smith, C. P., and Micklefield, J. (2002) Structure, biosynthetic origin, and engineered biosynthesis of calcium-dependent antibiotics from *Streptomyces coelicolor*, *Chem. Biol. 9*, 1175–1187.
10. Neary, J. M., Powell, A., Gordon, L., Milne, C., Flett, F., Wilkinson, B., Smith, C. P., and Micklefield, J. (2007) An asparagine oxygenase (AsnO) and a 3-hydroxyasparaginyl phosphotransferase (HasP) are involved in the biosynthesis of calcium-dependent lipopeptide antibiotics, *Microbiology 153*, 768–776.
11. Jensen, S. E., and Paradkar, A. S. (1999) Biosynthesis and molecular genetics of clavulanic acid, *Antonie van Leeuwenhoek 75*, 125–133.
12. Hausinger, R. P. (2004) FeII/alpha-ketoglutarate-dependent hydroxylases and related enzymes, *Crit. Rev. Biochem. Mol. Biol. 39*, 21–68.
13. Vaillancourt, F. H., Yin, J., and Walsh, C. T. (2005) SyrB2 in syringomycin E biosynthesis is a nonheme Fe^{II} alpha-ketoglutarate- and O_2-dependent halogenase, *Proc. Natl. Acad. Sci. U.S.A. 102*, 10111–10116.
14. Katz, E., Kamal, F., and Mason, K. (1979) Biosynthesis of trans-4-hydroxy-L-proline by *Streptomyces griseoviridus*, *J. Biol. Chem. 254*, 6684–6690.
15. Onishi, M., Okumura, Y., Okamoto, R., and Ishikura, T. (1984) Proline hydroxylation by cell free extract of a streptomycete, *Biochem. Biophys. Res. Commun. 120*, 45–51.
16. Yin, X., O'Hare, T., Gould, S. J., and Zabriskie, T. M. (2003) Identification and cloning of genes encoding viomycin biosynthesis from *Streptomyces vinaceus* and evidence for involvement of a rare oxygenase, *Gene 312*, 215–224.
17. Yin, X., and Zabriskie, T. M. (2004) VioC is a non-heme iron, alpha-ketoglutarate-dependent oxygenase that catalyzes the formation of 3S-hydroxy-L-arginine during viomycin biosynthesis, *ChemBioChem 5*, 1274–1277.
18. Grünewald, J., Sieber, S. A., and Marahiel, M. A. (2004) Chemo- and regioselective peptide cyclization triggered by the N-terminal fatty acid chain length: the recombinant cyclase of the calcium-dependent antibiotic from *Streptomyces coelicolor*, *Biochemistry 43*, 2915–2925.
19. Einarsson, S., Josefsson, S., and Lagerkvist, S. (1983) Determination of amino acids with 9-fluorenylmethyl chloroformate and reversed-phase high performance liquid chromatography, *J. Chromatogr. 282*, 609–618.
20. Kirschbaum, J., Luckas, B., and Beinert, W. D. (1994) Precolumn derivatization of biogenic-amines and amino-acids with 9-fluorenylmethyl chloroformate and heptylamine, *J. Chromatogr. A 661*, 193–199.
21. Müller, T. A., Fleischmann, T., van der Meer, J. R., and Kohler, H. P. E. (2006) Purification and characterization of two enantioselective alpha-ketoglutarate-dependent dioxygenases, RdpA and SdpA, from *Sphingomonas herbicidovorans* MH, *Appl. Environ. Microbiol. 72*, 4853–4861.
22. Zhang, Z., Ren, J., Stammers, D. K., Baldwin, J. E., Harlos, K., and Schofield, C. J. (2000) Structural origins of the selectivity of the trifunctional oxygenase clavaminic acid synthase, *Nat. Struct. Biol. 7*, 127–133.
23. Clifton, I. J., McDonough, M. A., Ehrismann, D., Kershaw, N. J., Granatino, N., and Schofield, C. J. (2006) Structural studies on 2-oxoglutarate oxygenases and related double-stranded beta-helix fold proteins, *J. Inorg. Biochem. 100*, 644–669.

24. Roach, P. L., Clifton, I. J., Fulop, V., Harlos, K., Barton, G. J., Hajdu, J., Andersson, I., Schofield, C. J., and Baldwin, J. E. (1995) Crystal structure of isopenicillin N synthase is the first from a new structural family of enzymes, *Nature 375*, 700–704.
25. Valegard, K., van Scheltinga, A. C., Lloyd, M. D., Hara, T., Ramaswamy, S., Perrakis, A., Thompson, A., Lee, H. J., Baldwin, J. E., Schofield, C. J., Hajdu, J., and Andersson, I. (1998) Structure of a cephalosporin synthase, *Nature 394*, 805–809.
26. Baldwin, J. E., Field, R. A., Lawrence, C. C., Merritt, K. D., and Schofield, C. J. (1993) Proline 4-hydroxylase: stereochemical course of the reaction, *Tetrahedron Lett. 34*, 7489–7492.
27. Sali, A., and Blundell, T. L. (1993) Comparative protein modelling by satisfaction of spatial restraints, *J. Mol. Biol. 234*, 779–815.
28. Bentley, S. D., Chater, K. F., Cerdeno-Tarraga, A. M., Challis, G. L., Thomson, N. R., James, K. D., Harris, D. E., Quail, M. A., Kieser, H., Harper, D., Bateman, A., Brown, S., Chandra, G., Collins, M., Cronin, A., Fraser, A., Goble, A., Hidalgo, J., Hornsby, T., Howarth, S., Huang, C. H., Kieser, T., Larke, L., Murphy, L., Oliver, K., O'Neil, S., Rabbinowitsch, E., Rajandream, M. A., Rutherford, K., Rutter, S., Seeger, K., Saunders, D., Sharp, S., Squares, R., Squares, S., Taylor, K., Warren, T., Wietzorrek, A., Woodward, J., Barrell, B. G., Parkhill, J., and Hopwood, D. A. (2002) Complete genome sequence of the model actinomycete *Streptomyces coelicolor* A3(2), *Nature 417*, 141–147.
29. Miao, V., Brost, R., Chapple, J., She, K., Gal, M. F., and Baltz, R. H. (2006) The lipopeptide antibiotic A54145 biosynthetic gene cluster from Streptomyces fradiae, *J. Ind. Microbiol. Biotechnol. 33*, 129–140.
30. Piepersberg, W. (2004) Directed deposit to GenBank (AJ810851.1).
31. Haltli, B., Tan, Y., Magarvey, N. A., Wagenaar, M., Yin, X., Greenstein, M., Hucul, J. A., and Zabriskie, T. M. (2005) Investigating beta-hydroxyenduracididine formation in the biosynthesis of the mannopeptimycins, *Chem. Biol. 12*, 1163–1168.
32. Ju, J., Ozanick, S. G., Shen, B., and Thomas, M. G. (2004) Conversion of (2S)-arginine to (2S,3R)-capreomycidine by VioC and VioD from the viomycin biosynthetic pathway of *Streptomyces* sp. strain ATCC11861, *ChemBioChem 5*, 1281–1285.
33. Price, J. C., Barr, E. W., Hoffart, L. M., Krebs, C., and Bollinger, J. M., Jr. (2005) Kinetic dissection of the catalytic mechanism of taurine: alpha-ketoglutarate dioxygenase (TauD) from *Escherichia coli*, *Biochemistry 44*, 8138–8147.
34. Hoffart, L. M., Barr, E. W., Guyer, R. B., Bollinger, J. M., Jr., and Krebs, C. (2006) Direct spectroscopic detection of a C-H-cleaving high-spin Fe(IV) complex in a prolyl-4-hydroxylase, *Proc. Natl. Acad. Sci. U.S.A. 103*, 14738–14743.
35. Lee, C., Kim, S. J., Jeong, D. G., Lee, S. M., and Ryu, S. E. (2003) Structure of human FIH-1 reveals a unique active site pocket and interaction sites for HIF-1 and von Hippel-Lindau, *J. Biol. Chem. 278*, 7558–7563.
36. Semenza, G. L. (1999) Regulation of mammalian O_2 homeostasis by hypoxia-inducible factor 1, *Annu. Rev. Cell Dev. Biol. 15*, 551–578.
37. Prescott, A. G., and Lloyd, M. D. (2000) The iron(II) and 2-oxoacid-dependent dioxygenases and their role in metabolism, *Nat. Prod. Rep. 17*, 367–383.
38. Kershaw, N. J., Caines, M. E., Sleeman, M. C., and Schofield, C. J. (2005) The enzymology of clavam and carbapenem biosynthesis, *Chem. Commun. (Cambridge) Sep 14*, 4251–4263.
39. Bridges, R. J., and Esslinger, C. S. (2005) The excitatory amino acid transporters: pharmacological insights on substrate and inhibitor specificity of the EAAT subtypes, *Pharmacol. Ther. 107*, 271–285.
40. Stein, D. B., Linne, U., and Marahiel, M. A. (2005) Utility of epimerization domains for the redesign of nonribosomal peptide synthetases, *FEBS J. 272*, 4506–4520.
41. CCP4 (1994) The CCP4 suite: programs for protein crystallography, *Acta Crystallogr. D50*, 760–763 .
42. Vagin, A., and Teplyakov, A. (1997) MOLREP: an automated program for molecular replacement, *J. Appl. Crystallogr. 30*, 1022–1025.
43. Murshudov, G. N., Vagin, A. A., and Dodson, E. J. (1997) Refinement of macromolecular structures by the maximum-likelihood method, *Acta Crystallogr. D 53*, 240–255.
44. Emsley, P., and Cowtan, K. (2004) COOT: model-building tools for molecular graphics, *Acta Crystallogr. D 60*, 2126–2132.
45. DeLano, W. L. DeLano Scientific LLC, San Carlos, CA, 2002.